INSTITUTE OF PHYSICS PUBLISHING JOURNAL OF MICROMECHANICS AND MICROENGINEERING

J. Micromech. Microeng. **14** (2004) 1270–1279 PII: S0960-1317(04)79890-3

Effect of temperature on capacitive RF MEMS switch performance—a coupled-field analysis

Yong Zhu and Horacio D Espinosa

Department of Mechanical Engineering, Northwestern University, Evanston, IL 60208-3111, USA

E-mail: espinosa@northwestern.edu

Received 27 April 2004
Published 21 June 2004
Online at stacks.iop.org/JMM/14/1270
doi:10.1088/0960-1317/14/8/021

Abstract

Three-dimensional multiphysics finite element analysis (FEA) was performed to investigate the reliability of RF MEMS switches at various operational temperatures. The investigated MEMS capacitive switch consists of a freestanding metal membrane actuated by a bottom electrode coated by a dielectric film. Coupled-field simulations between thermal, structural and electrostatic domains were performed. The simulations show that temperature significantly changes both the membrane stress state and out-of-plane geometry. In particular, the membrane buckles when temperature increase, from room temperature, takes place. The buckling temperature, i.e. the upper bound to the operational temperature, is a function of manufacturing residual stress state, membrane initial out-of-plane profile and a mismatch in materials coefficient of thermal expansion. The analysis also shows that temperature reduction, from room temperature to −40 °C, causes an increase in pull-in voltage to values that could compromise the switch reliability as a result of charge build-up in the dielectric layer. Our analyses illustrate that by proper designing of the membrane out-of-plane profile, it is possible to keep the pull-in voltage, at all operational temperatures, within allowable values. This design feature of RF MEMS switches offers an effective way to achieve reliable pull-in voltages in applications where large temperature variations are expected such as in satellites and airplane condition monitoring based on wireless communication.

(Some figures in this article are in colour only in the electronic version)

1. Introduction

Microelectromechanical systems (MEMS) technology is on the verge of revolutionizing radio frequency (RF) and microwave applications. Several universities and companies [1–6] have developed RF MEMS switches during the last decade, which demonstrated outstanding RF performance from dc to 100 GHz. Most of these switches are electrostatically actuated because of their low power consumption and bias networking simplicity.

Despite these advantages, the reliability of MEMS switches is of major concern for long-term and broad applicability. For capacitive coupling switches, the long-term reliability is limited by stiction between the metal layer and the dielectric layer due to charge build-up in the dielectric material. By contrast, mechanical fatigue or fracture is less important [7]. This has been shown to be a case by means of extensive on-chip experimentation [8]. This charge build-up is dependent on the actuation voltage. It was shown that a reduction in the actuation voltage by 6 V results in a ten-fold increase in the lifetime of typical capacitive MEMS switches [9]. Therefore, it is essential to achieve low actuation voltages, at all operational temperature, from a reliability and performance viewpoint.

In applications where significant temperature variations are expected, such as in aircraft condition monitoring and distributed satellites communication, as well as during device packaging [10, 11], the effect of temperature on the device performance is a major concern. Preliminary results have been reported on the effects of temperature on MEMS switches pull-in voltage [12]. This study shows that a moderate temperature increase may cause buckling of the switch structure, leading to premature failure of the device. Tensile residual stress has been found to increase the buckling critical temperature; however, the required residual stress may significantly increase the actuation voltage at other operational temperatures. In fact, a significant temperature drop from room temperature may result in device pull-in voltages outside the reliable range. These features illustrate the need for identifying switch structures that are able to decrease the device sensitivity to temperature variations while maintaining a reliable actuation voltage. Besides environmental temperature changes, temperature changes due to power dissipation can equally affect switch reliability [13, 14]. In this context, thermo-electrostatic-structural coupled simulations are required in the design and optimization of switch structure.

It is the purpose of this paper to present an analysis methodology and our findings on this issue. Our three-dimensional (3D) finite element analysis (FEA) starts with a thermo-mechanical analysis to identify the equilibrated switch geometry, in particular its new out-of-plane profile and in-plane thermal stress. This new geometry and corresponding stress state are used as the starting point of the subsequent electrostatic–structural analysis, which in turn calculates the actuation voltage at a given operational temperature. The paper is organized as follows: (1) thermo-electrostatic-mechanical coupled analysis of investigated capacitive RF switches is discussed; (2) a 3D FEA model, including nonlinear strain tension stiffening effect, is presented; this model is more general than those previously reported in the literature and can be employed in the investigation of many types of electrostatically actuated MEMS devices; (3) simulation results and discussion of the effects of membrane out-of-plane geometry, residual stress state and temperature on device pull-in voltage are presented; (4) concluding remarks on the reliable design of RF MEMS devices are summarized.

2. Thermo-electro-mechanical analysis of RF MEMS switches

2.1. Capacitive MEMS switch operation

A typical capacitive RF MEMS switch consists of a fixed–fixed thin metallic membrane suspended over a bottom electrode insulated by a dielectric film, as illustrated in figure 1. This dielectric film serves to prevent the electric short between two conductors and provides a low impedance path for the RF signal. When the switch is unactuated, there is a low capacitance between the membrane and the bottom electrode, and the device is in the off state. When an electrostatic voltage between the two conductors is applied, an electrostatic force is created to pull the membrane down. At a certain voltage, the so-called pull-in voltage, the membrane collapses and makes a contact with the dielectric layer. The device is in the on state, and its capacitance is much larger than that in the off state [2, 8].

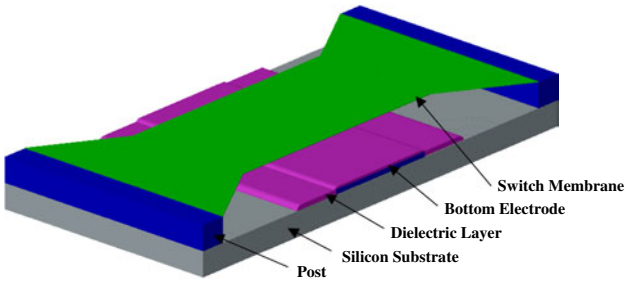

Figure 1. Schematic of a capacitive RF MEMS switch.

When a voltage is applied between the flexible structure and the fixed bottom electrode, electrostatic charges are induced on both the structure and the bottom electrode. The electrostatic charges cause a distributed electrostatic force, which deforms the flexible structure. In turn, such a deformation leads to storage of elastic energy, which tries to restore the structure to its original shape. The structure deformation also results in the reorganization of all surface charges on the device. This reorganization of charges causes further structural deformation; hence, the device exhibits a highly nonlinear-coupled electromechanical behavior. Up to a certain applied voltage, an equilibrium position exists through a balance between the elastic restoring force and electrostatic force. In addition, if a change in operational temperature occurs, the coupled behavior of the MEMS switch varies because the membrane geometry and stress state are altered. Therefore, a full thermo-electro-mechanical analysis is required in identifying pull-in voltage and its implication on the device performance.

2.2. The coupled-field problem

Usually a MEMS switch has a certain out-of-plane waviness [5, 15, 16] and associated state of residual stress. The out-of-plane profile changes significantly with temperature, though change in the in-plane shape is negligible. Likewise, the stress state in the switch changes as a result of the device thermal deformation.

In analyses discussed here, the membrane geometry and stress state at the operational temperature are the starting point for the subsequent electrostatic–structural coupled analysis. Given the potentials on the conductors, the potential distribution is calculated by an electrostatic analysis. The problem can be described by *Laplace*'s equation with two known potential boundary conditions, namely

$$\nabla^2 V = \frac{\partial^2 V}{\partial x^2} + \frac{\partial^2 V}{\partial y^2} + \frac{\partial^2 V}{\partial z^2} = 0 \qquad (1a)$$

$$V = V_0 \quad \text{at the switch membrane (top electrode)} \qquad (1b)$$

$$V = 0 \quad \text{at bottom electrode} \qquad (1c)$$

where V denotes the potential distribution in the medium (such as air and vacuum) surrounding the two electrodes, and V_0 is the applied voltage on the top electrode. This equation is

suitable to any configuration of the switch, not necessarily a flat one.

On the other hand, the switch deformation due to the electrostatic force can be calculated following the theory of plates and shells. The switch membrane is a thin shell, elastic, homogeneous and isotropic, from a mechanics viewpoint. For the case of a capacitive coupling MEMS switch, the deflection is several times larger than the thickness but the state of stress does not reach material yielding. Therefore, a nonlinear strain stiffening effect has to be included. It is known that this nonlinear effect significantly increases the pull-in voltage [17]. In the 2D case, the nonlinear deflection can be described by the *von Karman* equation [18]:

$$\frac{\mathrm{d}^4 w}{\mathrm{d}x^4} = \frac{1}{D}\left[-\frac{\varepsilon V_0^2}{2(g_0 - w)^2} + \frac{Et}{2}\left(\frac{\mathrm{d}w}{\mathrm{d}x}\right)^2\left(\frac{\mathrm{d}^2 w}{\mathrm{d}x^2}\right) + \sigma_0(1-\nu)t\left(\frac{\mathrm{d}^2 w}{\mathrm{d}x^2}\right)\right] \tag{2a}$$

$$w = 0|_{x=\pm L/2} \qquad \text{and} \qquad \frac{\partial w}{\partial x} = 0|_{x=\pm L/2} \tag{2b}$$

where $D = \frac{Et^3}{12(1-\nu^2)}$ is the flexural rigidity of the plate, E is the Young's modulus, t is the plate thickness, g_0 is the initial gap, σ_0 is the biaxial residual stress presumed present before the membrane shape is etched [19], ν is the Poisson ratio and $\sigma_0(1-\nu)$ is the approximate resulting uniaxial stress. The first term on the right-hand side of equation (2*a*) arises from the electrostatic force, the second term originates from nonlinear strain stiffening and the third term derives from the residual stress. The electrostatic fringing field is here neglected since the gap is much smaller than the width. The small deformation version of equation (2*a*) was used in the analysis of the M-test [19].

For details on the electrostatic–structural coupled analysis, please refer to [17, 19, 20]. Though in principle this problem can be solved in both domains by integrating equations (1) and (2) simultaneously, in reality the problem is complicated to such a degree that it cannot be solved in a closed form. For instance, the geometry of the switch could be a bow tie [2], the out-of-plane profile not necessarily flat [5, 15, 16] and a nonuniform state of residual stress, resulting from the microfabrication process, present in the device [16, 21]. What makes it even more complicated is that the switch geometry and residual stress state are both functions of temperature. In this paper, we use the finite element method to solve the coupled-field problem.

3. Finite element modeling

The performance of MEMS switches under different temperatures was simulated using the finite element software ANSYS Multiphysics, version 6.1. The simulation consisted of two steps in sequence: thermo-structural analysis and electrostatic–structural analysis. First the solid model consisting of the switch, the bottom electrode and the surrounding medium was developed. Two physical environments, electrostatic and structural environments, were defined based on the solid model and boundary conditions.

The thermo-mechanical analysis was performed within the structural environment. A uniform temperature was applied to the device, and the thermal expansion coefficient used for the membrane was assumed to be the difference between that for the membrane and the substrate. In the analyses, a silicon substrate and an aluminum membrane were modeled. The thermo-mechanical analysis resulted in a new switch geometry, especially its out-of-plane profile, and nonuniform in-plane thermal stresses. This new geometry and new stress state were used as the starting point for the electrostatic–structural analysis.

The electrostatic–structural analysis was performed as a sequentially coupled analysis involving a two-way coupling between both the electrostatic and structural environments. In the electrostatic environment, the boundary condition was the applied voltage on both top and bottom conductors. By solving Laplace's equation, the voltage distribution in the surrounding medium was obtained and the electrostatic force between the two conductors was calculated. Then, the analysis environment was switched to the structural environment. A new deformation state was obtained arising from the electrostatic force. The analysis was switched back to the electrostatic environment, and the electrostatic mesh was updated according to the updated membrane geometry. Iterations between these two physical environments were executed in a sequence until a convergence in both environments was reached. This process was repeated for every applied voltage. The pull-in voltage was identified when a convergent solution was not achievable. This voltage corresponds to the start of unstable regime of the switch.

Since the thickness of the switch is far smaller than its length and width, shell elements were employed to model the switch freestanding membrane (figure 2(*a*)). Solid elements were used to model the surrounding medium to account for the electrostatic field. In view that the model is symmetric, with respect to both x and y axes, only a quarter of the switch was model (figure 2(*b*)). The mesh in purple represents the surrounding medium, while that in green (embedded) is the switch membrane. It is noted that the bottom electrode was not meshed, since it did not deform and only served as a voltage boundary condition. From environment to environment, the element types were changeable. For instance, in the electrostatic environment, the element type for the membrane was the so-called 'null', equivalent to the absence of electrostatic field inside the structure, and that of the surrounding medium was electrostatic 122. By contrast, in the structural environment, the element type for the membrane was defined as shell 93, and that of the surrounding was defined as 'null'.

To assess the accuracy of the FEA model, two examples of the electrostatic–structural coupled analysis were performed. The first example was designed to compare with an analytical solution. A flat rectangular plate, with dimensions 320 μm long, 100 μm wide and 0.3 μm thick, supported by a spring was used. The system is a lumped model of a switch with linear structural behavior. The analytical solution for this model is given by [20]

$$V(w) = \sqrt{\frac{2k}{\varepsilon A}(g_0 - w)^2 w} \tag{3}$$

where g_0 is the initial gap between the upper and bottom plates (4 μm), w is the deflection, k is the spring stiffness (0.14 N m^{-1}) and A is the plate area.

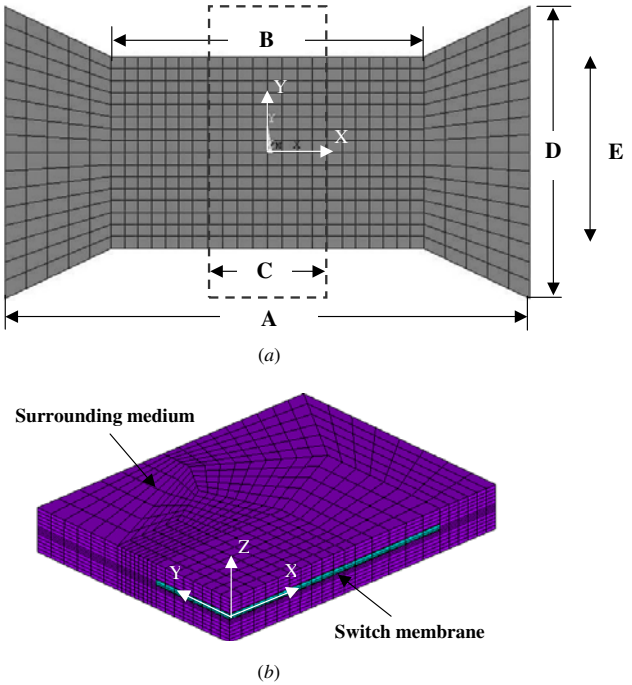

Figure 2. (*a*) Mesh of the switch freestanding membrane with dimensions A = 320 μm, B = 190 μm, C = 90 μm, D = 180 μm and E = 100 μm, as used in the simulation. The membrane thickness is 300 nm, and the gap between the membrane and the bottom electrode is 4 μm. The dashed-line box shows the bottom electrode, whose width is equal to the switch edge width. (*b*) A quarter of the meshed model including the embedded switch membrane (structure) and surrounding medium (electrostatic field). The bottom electrode was not meshed in the simulation.

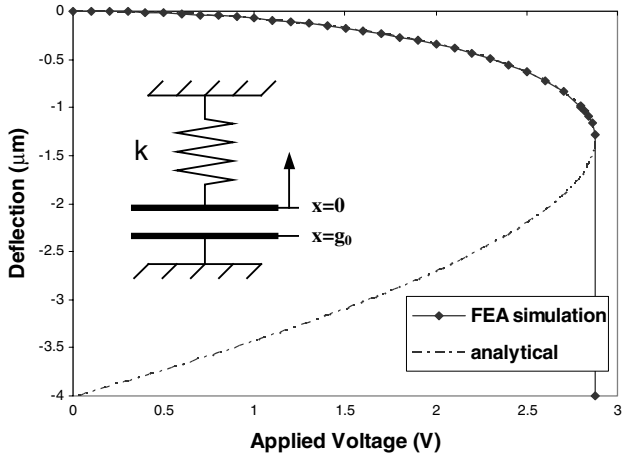

Figure 3. Deflection–applied voltage curves for parallel-plate-linear spring system from analytical solution and 3D FEA model. Inset is the parallel-plate with a linear spring.

The analytical and the FEA simulation results are shown in figure 3. The analytical pull-in is given by $V_{\text{pull-in}} = \sqrt{\frac{8k}{27\varepsilon A}} g_0^3$, which is 2.87 V in this example. By comparison, the pull-in voltage from the FEA simulation is 2.8 V. This example illustrates the accuracy of the stagger-coupled analysis.

The second example consisted in the analysis of a polychromator grating structure reported in [20]. The numerical results were compared to the published experimental data. The structure consisted of a fixed–fixed beam and two bottom electrodes. The beam was 500 μm long, 10 μm wide and 2 μm thick. The bottom electrode was 80 μm long and 10 μm wide. The nominal gap was 2 μm. The residual stress for this type of structure was characterized as nearly zero. The nonlinear strain stiffening effect was considered in the simulation. Figure 4 shows the geometry of the polychromator grating structure and a plot of center deflection versus applied voltage. An agreement between the simulation and the experimental data is evident.

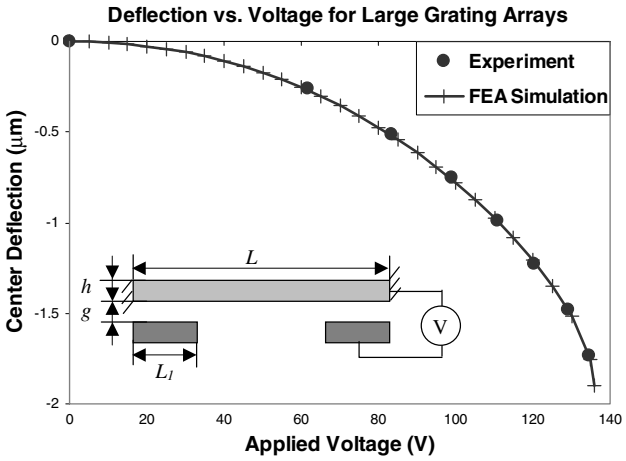

Figure 4. Center deflection–applied voltage curve for a polychromator grating structure. The experimental data are from [20]. Inset is the structure geometry. Parameters used for simulation: $L = 500$ μm, $L_1 = 80$ μm, $h = 2.21$ μm, $g = 2.05$ μm and $\sigma_0 = 0$, using measured film thickness.

Table 1. RF switch material properties used in the simulation [7].

Material property	Value
Thermal expansion coefficient of Al (10^{-6} K^{-1})	23.1
Thermal expansion coefficient of Si (10^{-6} K^{-1})	2.6
Young's modulus of Al (GPa)	70
Poisson ratio of Al	0.35

Given the good accuracy exhibited by the coupled finite element analysis, in the next section the FEA model is applied to the analysis of a bow tie switch with various out-of-plane profiles and temperature states.

4. Results and discussion

The effect of temperature on the performance of MEMS capacitive switches can be associated with the change in membrane out-of-plane profile and stress state. The residual stress state in a MEMS device is due to temperature changes at various steps in the microfabrication process and to intrinsic strains. In this section, we begin by examining the effect of residual stress state followed by the effect of out-of-plane profiles on pull-in voltage. Next, the effect of temperature is examined in terms of pull-in voltage, membrane geometry and stress state. The material properties for the switch membrane examined here are listed in table 1. The material properties are isotropic in all directions.

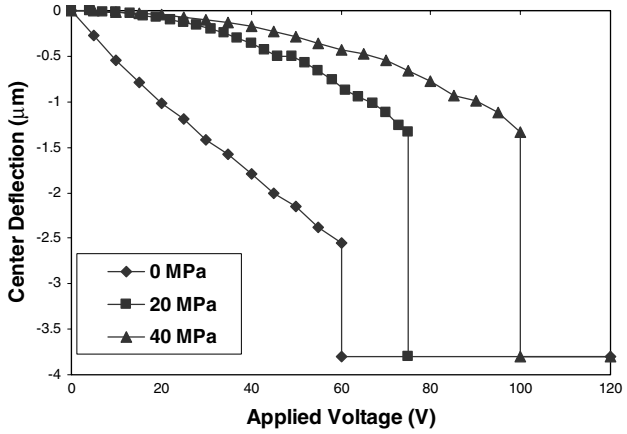

Figure 5. Center deflection–applied voltage curves of a bow tie shaped flat switch with and without residual stresses. Note that the tensile residual stress significantly increases the pull-in voltage as expected from tension stiffness effects.

4.1. Effects of residual stress

Residual stress is inherently introduced during microfabrication. Due to the fixed–fixed structure of capacitive switches, in-plane stresses may result in buckling of the device or tension stiffness. In general, only micromachining processes resulting in tensile stress in the thin film can be employed [2]. In this section, we will only consider the effect of tensile residual stresses. The tensile stress in RF switches usually ranges from a few MPa to over 100 MPa [21]. 20 MPa and 40 MPa uniaxial tensile stresses were applied to the bow tie shaped switch to examine its effect on pull-in voltage. For simplicity, the switch membrane was assumed flat and without holes. The center deflection–applied voltage curves predicted by the analyses are shown in figure 5. It can be seen that the tensile residual stress increases the pull-in voltage and that values in excess of 100 V are needed when the residual stress is 40 MPa. It is known that this high actuation voltages typically result in switch failure after a limited number of actuation cycles. The failure occurs because of charge build-up in the dielectric layer. Therefore, designing of reliable MEMS switches requires much lower actuation voltages. Two strategies have been proposed in the literature to achieve this goal. One consists in the addition of holes in the membrane such that a reduced equivalent Young's modulus is obtained [22, 23]. The second consists in modifying the out-of-plane geometry of the membrane such that the switch structure is much more compliant [5, 15, 16, 24, 25]. This effect is the most dominant; hence, it is examined in detail in the next subsection. In applications, both strategies are employed concomitantly.

4.2. Effects of out-of-plane profile

A switch membrane out-of-plane profile is achievable by proper selection of microfabrication processes [5, 15]. Such a profile significantly affects the thermo-electro-mechanical performance of the switch. Two arbitrary profiles are examined in addition to the flat membrane (figure 6(*a*)). Profiles A and B are described, respectively, by the following functions:

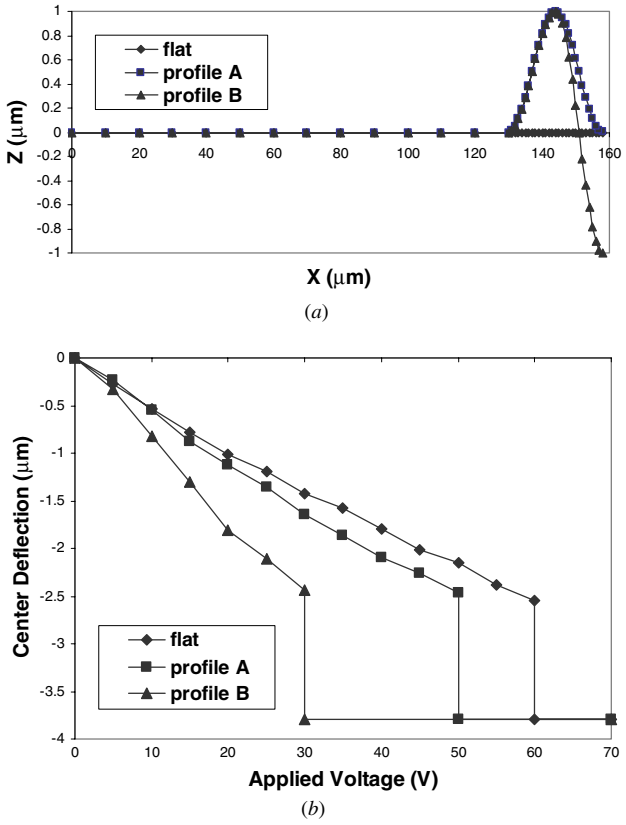

Figure 6. (*a*) Out-of-plane profiles used to examine switch performance. Due to symmetry only half of the profile is shown. (*b*) Comparison of center deflection–applied voltage curves for flat and profiles A and B as defined by equations (4) and (5).

profile A:

$$z = 0 \qquad \text{when} \qquad |x| \leqslant \frac{A+B}{4} \tag{4a}$$

$$z = \frac{1}{2}\left\{\sin\left[\frac{8\pi}{A-B}\left(|x| - \frac{5A+3B}{16}\right)\right] + 1\right\}$$
$$\text{when} \qquad \frac{A+B}{4} \leqslant |x| \leqslant \frac{A}{2} \tag{4b}$$

profile B:

$$z = 0 \qquad \text{when} \qquad |x| \leqslant \frac{A+B}{4} \tag{5a}$$

$$z = \frac{1}{2}\left\{\sin\left[\frac{8\pi}{A-B}\left(|x| - \frac{5A+3B}{16}\right)\right] + 1\right\}$$
$$\text{when} \qquad \frac{A+B}{4} \leqslant |x| \leqslant \frac{3A+B}{8} \tag{5b}$$

$$z = \sin\left[\frac{8\pi}{A-B}\left(|x| - \frac{5A+3B}{16}\right)\right]$$
$$\text{when} \qquad \frac{3A+B}{8} \leqslant |x| \leqslant \frac{A}{2}. \tag{5c}$$

Parameters A and B are defined in figure 2(*a*). Figure 6(*b*) shows the center deflection–applied voltage curves for the two out-of-plane profiles and the flat membrane. It can be seen that out-of-plane profile reduces the pull-in voltage dramatically, especially in the case of profile B. In these analyses, a zero state of residual stress was considered.

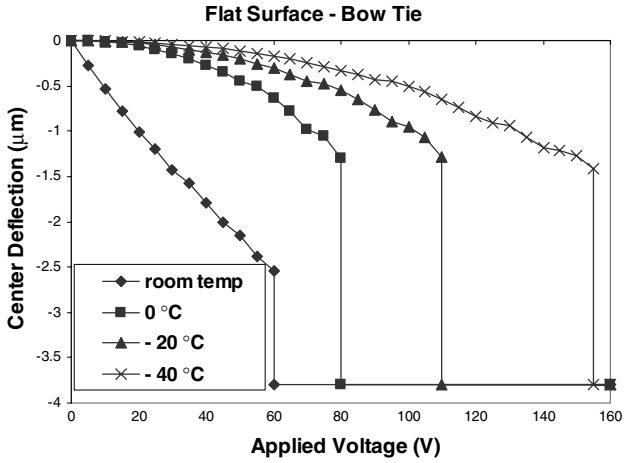

Figure 7. Center deflection–applied voltage curves for a bow tie shaped flat switch at different operational temperatures. It is observed that a temperature reduction dramatically increases the pull-in voltage to values in excess of 150 V.

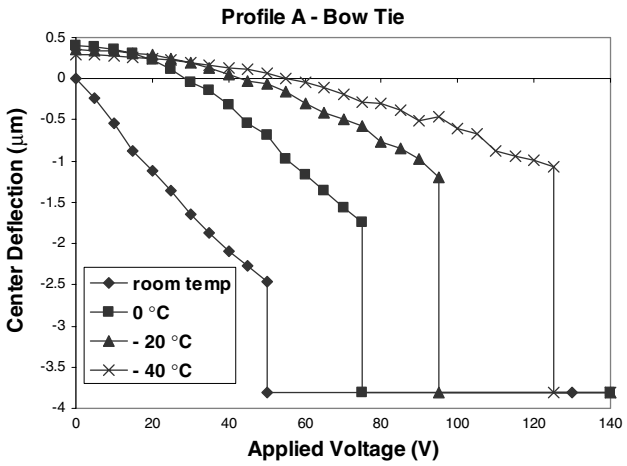

Figure 8. Center deflection–applied voltage curves for a bow tie shaped switch with out-of-plane profile A. At −40 °C the pull-in voltage exceeds 120 V.

4.3. Effects of temperature

The effect of operational temperature on switch behavior is shown in figures 7, 8 and 9 for flat, profiles A and B, respectively. It is observed that in all cases a temperature reduction from room temperature dramatically increases the pull-in voltage. The pull-in voltages for these three profiles as a function of temperature are plotted in figure 10. By comparing flat membrane with out-of-plane profiles A and B, it can be observed that the out-of-plane profile controls the increase in pull-in voltage to a certain degree. Profile A has a limited effect in controlling the pull-in voltage. By contrast, profile B has a more beneficial effect. Ideally, the designer would like to obtain a temperature independent pull-in voltage. Profile B does not reach such a level of performance but exhibits only a moderate increase in pull-in voltage as temperature drops to −40 °C. It is therefore inferred that with the addition of membrane holes, profile B possesses pull-in voltages that could be advantageously implemented in practical applications.

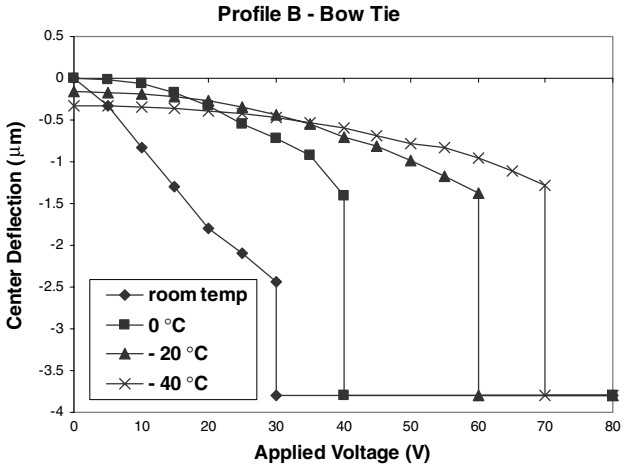

Figure 9. Center deflection–applied voltage curves for a bow tie shaped switch with out-of-plane profile B.

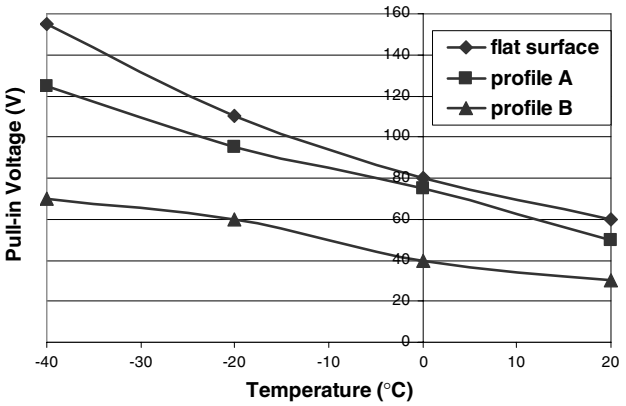

Figure 10. Pull-in voltages for three out-of-plane profiles at different temperatures.

How temperature changes affect the device pull-in voltage can be explained from examining two features: a variation in membrane out-of-plane profile and resulting residual stresses before actuation of the switch. A temperature change, from room temperature, results in membrane geometry and thermal stress state changes. Hence, by analyzing the evolution of the membrane geometry and its stress state, insight into these effects is gained. Figure 11 shows the stress state and change of profile for both flat and profile A membranes as a result of a temperature reduction from room temperature to −20 °C. For a flat membrane, there is no out-of-plane profile change because the membrane develops tensile stresses when temperature is reduced. Moreover, the average Cauchy stress in the *X*-direction, in the constant width region, reaches a value of about 70 MPa; by contrast, the average Cauchy stress in the *X*-direction, in the whole membrane, is 64 MPa. The thermal stress is nonuniform due to the bow tie configuration. For profile A, the average Cauchy stress in the *X*-direction, in the same region, is about 31 MPa. It should be noted that the state of stress is highly nonuniform in the regions close to the supports where the out-of-plane amplitude is the largest. Note also that the out-of-plane profile changes significantly with temperature, figure 11(*c*). The towers near the edges are displaced down, while the central part is displaced up.

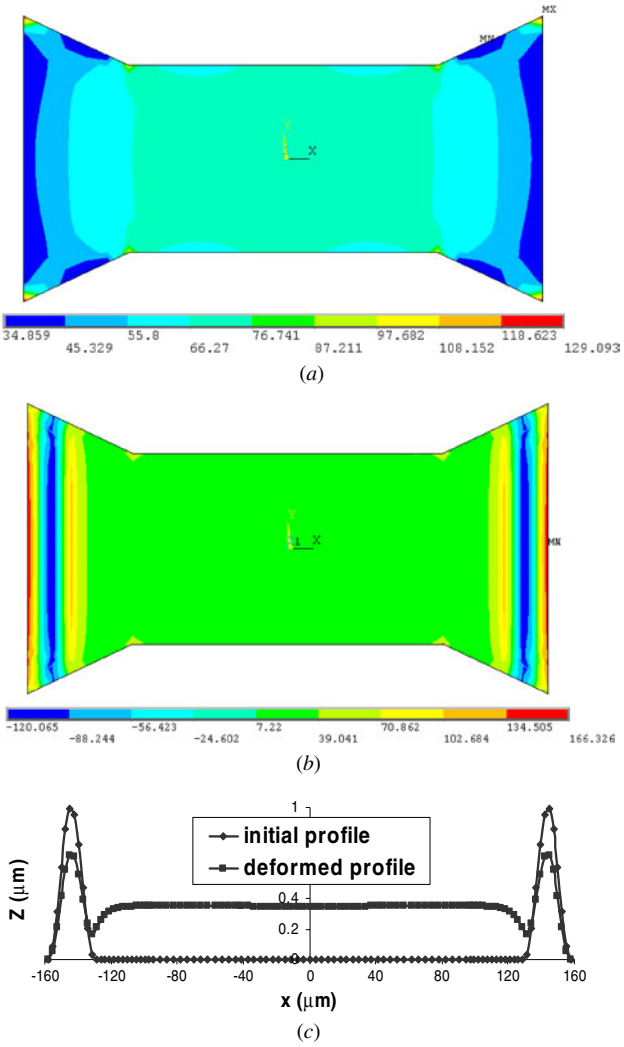

Figure 11. (*a*) Contours of Cauchy stress Sx for flat membrane at −20 °C before actuation (average stress 70.1 MPa); (*b*) Contours of Cauchy stress Sx for membrane with profile A at −20 °C before actuation (average stress 30.9 MPa); (*c*) change of switch profile as temperature is dropped from room temperature to −20 °C. The reader should note: (1) average stresses in all the figures in this paper are the average stress at the constant width region; (2) the *x* and *Z* scales are not one to one, to visually enhance the representation of the out-of-plane profiles.

By comparing flat and profile A membranes, it is observed that the profile A membrane effectively prevents a significant increase in in-plane stresses, which is the primary cause for the increase in pull-in voltage. It should also be noted that profile A changed to a configuration with a slight increase in the gap between membrane and bottom electrode, which in turn also increases the pull-in voltage. This explains why profile A exhibits only a small net improvement, in terms of pull-in voltage as a function of temperature, as compared to the flat membrane (figure 10).

As mentioned in the discussion of figure 10, from a design viewpoint, profile B is preferred because its pull-in voltage does not change as much when temperature is dropped to −40 °C. To understand why this is the case, we again follow the evolution of membrane in-plane stress state and out-of-plane profile with temperature drop. Figures 12(*a*), (*b*) and (*c*)

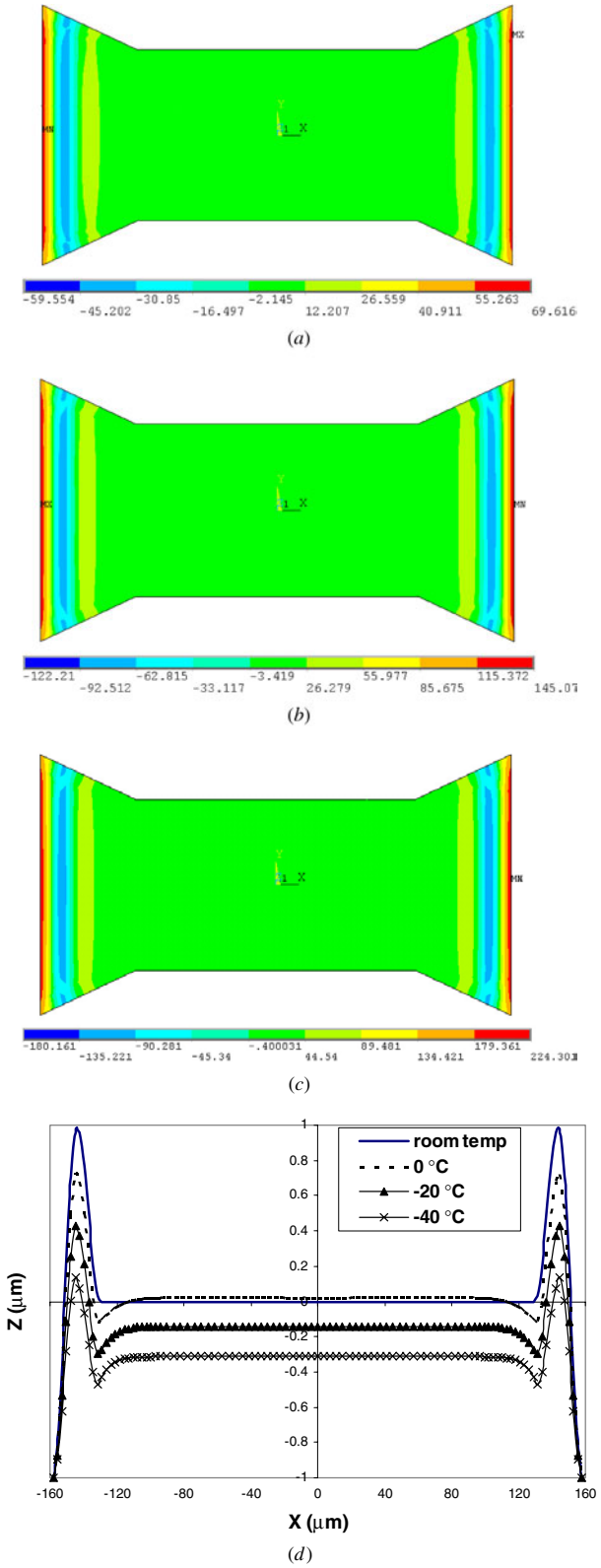

Figure 12. (*a*)–(*c*) Contours of Cauchy stress Sx for membrane with profile B at temperatures of 0 °C (average stress 6.5 MPa), −20 °C (average stress 16.5 MPa) and −40 °C (average stress 31.0 MPa), respectively. (*d*) Out-of-plane profile evolution from room temperature to −40 °C.

show the Cauchy stress contours in the *X*-direction for profile B at 0 °C, −20 °C and −40 °C, respectively. The stress

state is nonuniform. However, the average stress value in the flat region is about 6.5 MPa at 0 °C, 16.5 MPa at −20 °C and 31 MPa at −40 °C. This clearly indicates that a temperature reduction increases the overall in-plane tensile stress to a magnitude similar to those predicted in profile A. However, the evolution of the out-of-plane profile as a function of temperature (figure 12(*d*)) is quite different. A close comparison between the out-of-plane profiles for the 0 °C and −20 °C cases shows that the membrane deformed upwards slightly at 0 °C, but deformed downwards at −20 °C. As a result, the gap at 0 °C was larger than that at −20 °C, which would cause a comparatively larger pull-in voltage at 0 °C. On the other hand, the average stress value is 6.5 MPa at 0 °C and 16.5 MPa at −20 °C; the combination of these two affects resulted in larger pull-in voltage at −20 °C (figure 10). Similarly for the case of −40 °C, the membrane further deformed downwards and at the same time the average tensile stress increased to 31 MPa. The pull-in voltage increased to about 70 V as a result. There are two main advantages of profile B over flat and profile A membranes: (1) with temperature reduction, the gap between membrane and bottom electrode reduces, which helps to reduce pull-in voltage, though this gap reduction is small (less than 10% of initial gap); (2) tensile stress build-up due to the drop in temperature is considerably reduced.

These results show that an initial membrane out-of-plane profile limits the build-up of thermal stresses resulting from temperature variations. They also show that for a membrane out-of-plane profile to be effective, it needs to preserve the gap between the membrane and bottom electrode at all operational temperatures.

In all the above analysis, the microfabrication residual stress was assumed to be zero. In such a case, when the temperature increases, a compressive stress is introduced. Due to the membrane geometry, especially its thickness of just 0.3 μm, the switch membrane is easily buckled when a small temperature increase, above room temperature, occurs. However, this premature buckling can be avoided by a design and microfabrication process resulting in tensile residual stresses [12]. In fact, the tensile stress in capacitive RF switches usually ranges from a few MPa to over one hundred MPa [21]. In our analysis of this phenomenon, a 40 MPa uniform uniaxial tensile stress was set as initial condition for a membrane with profile B. Note that this stress is an initial stress used in the calculation and does not represent a real stress state satisfying equilibrium and compatibility. It is just a computational mean of achieving some desired level of residual stress state [16]. The membrane equilibrium stress state and corresponding compatible profile, at room temperature, are shown in figures 13(*a*) and (*b*), respectively. It is seen that the profile relaxes the applied stress significantly in the constant width region with an average stress of 10 MPa. As temperature increases, the membrane displaces upward while the tensile stress decreases; by contrast, as temperature decreases, the membrane displaces downward while the tensile stress increases. When the temperature reaches 50 °C, the membrane buckles as shown in figure 13(*b*). Above 50 °C, the stress state in the membrane changes from tension to compression. Figure 13(*c*) shows the pull-in curves at both high and low temperatures given this residual stress state. The

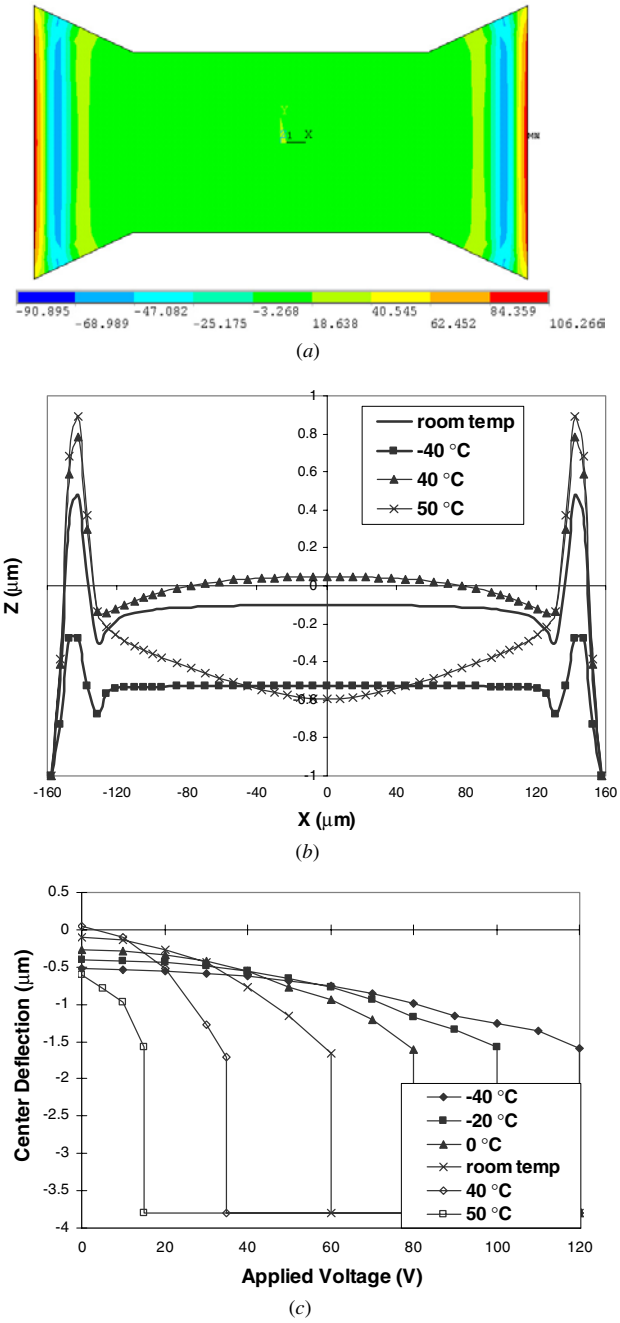

Figure 13. (*a*) Contours of Cauchy stress Sx for profile B at room temperature after an initial uniaxial stress is applied (average stress 10.1 MPa); (*b*) plot of switch profile evolution as temperature varies from −40 °C to 50 °C, at 50 °C, the membrane buckles; (*c*) pull-in curves from −40 °C to 50 °C. Note that the initial uniform uniaxial stress of 40 MPa, applied at room temperature, results in the equilibrated nonuniform stress distribution shown in (*a*) and a new compatible out-of-plane profile shown in (*b*).

highest reliable functional temperature in this case is 50 °C. In order to increase the functional temperature range, higher residual tensile stresses, introduced in the microfabrication proves, are required. Figure 14 plots the pull-in voltage versus temperature for three levels of residual stress. Here the residual stress and associated membrane shape are obtained following the procedure described above and in [16]. The residual stresses are the average stresses in the constant width

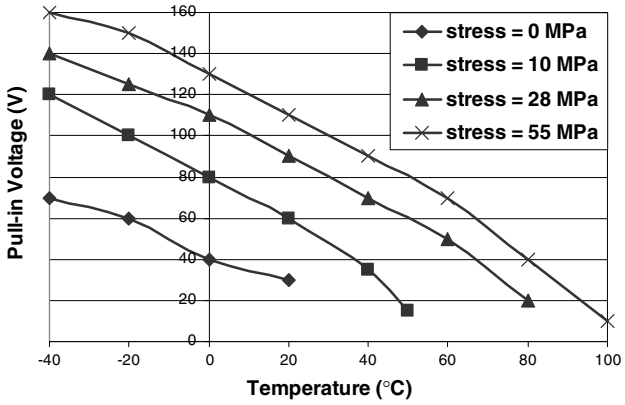

Figure 14. Pull-in voltages for three tensile residual stresses at different temperatures. The stress values represent the average stresses in the constant width region after stress relaxation.

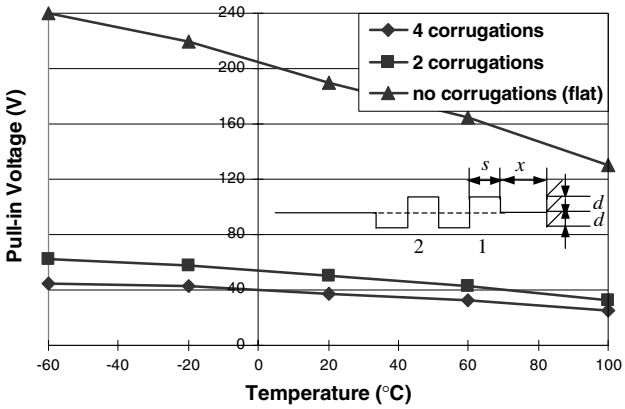

Figure 15. Pull-in voltages for three out-of-plane profiles, flat, corrugated membrane with two and four corrugations at each clamped edge, as a function of temperature. Inset shows the schematic of a switch membrane with two corrugations. The corrugation depth d is 1 μm, corrugation spacing s is 4 μm and distance from the anchor x is 5 μm. The membrane is rectangular with 320 μm length, 100 μm width and 0.3 μm thickness.

region of the membrane. For the case in which the residual stress is 55 MPa, the highest functional temperature is 100 °C. In brief, the reliable highest temperature of a MEMS switch is highly dependent on the microfabrication residual stress state. While high tensile residual stress leads to higher operational temperature, its effect may be detrimental at low operational temperatures as shown in figure 14. This trade-off needs to be kept in mind in the design of reliable MEMS capacitive switches.

A promising alternative to the out-of-plane profiles analyzed above is corrugated membranes. Corrugated membranes have been used successfully in pressure sensor to reduce the membrane stiffness and to increase its linear operation range [26]. The temperature response of corrugated membranes in RF MEMS switches has been analyzed in detail by us in [10]. The analyses are based on the finite element analysis described in this paper. The use of corrugated membranes has shown promising features in achieving reliable pull-in voltages over a broad temperature range. Figure 15 summarizes the findings reported in [10] on corrugated membranes.

5. Concluding remarks

A major obstacle in the commercialization of MEMS devices is their reliability at high and low temperatures. The modeling device performance is important to better understand the effects of device geometry, materials and microfabrication processes on its operation as a function of temperature. What is more important, the modeling provides valuable insight into the purpose of device design and optimization.

In this paper, a methodology for a coupled-field FEM analysis was presented to examine the performance of RF MEMS switches as a function of temperature. Likewise, the structure out-of-plane profile was investigated in detail. The main conclusions from these analyses are summarized as follows:

1. A general 3D thermo-electrostatic-structural FEA model can be employed to accurately investigate the behavior of MEMS switches at various temperatures. Such a model is suitable for any in-plane shape (not only rectangular or circular), arbitrary out-of-plane profile and residual stress state,
2. In-plane tensile stresses, arising from device microfabrication and temperature changes, may result in a significant increase in the pull-in voltage. The increase is highly dependent on the membrane out-of-plane profile.
3. The temperature increase introduces compressive stresses into the switch membrane that leads to buckling and device failure. In this context, tensile residual stresses are desirable for keeping the switch functioning reliably up to a certain temperature. The highest functional temperature depends on the value of the residual stress and out-of-plane profile. However, the tensile stresses may cause excessively high pull-in voltages at low temperatures.
4. The membrane out-of-plane profile has been identified as an effective mean to control stress relaxation and to achieve MEMS structures that are less sensitive to temperature variation while maintaining a suitable actuation voltage. The out-of-plane profile need be tailored to keep the pull-in voltage within optimal values for both low and high temperatures. Corrugated membranes appear to be very promising in this respect.

In conclusion, we note that optimization of out-of-plane profile needs to be further explored especially through device microfabrication and on-chip experimentation [16, 19]. It remains to be established how microfabrication processes can be selected such that the profiles here analyzed can be obtained in practice. The membrane corrugation, at a distance from the support area, is achievable with standard microfabrication processes and therefore may be the best choice.

Acknowledgments

The authors acknowledge the support from the FAA through award no DTFA03-01-C-00031 and the NSF through award no CMS-0120866. We would like to express our appreciation to Drs J Newcomb and J Larsen-Base for supporting this work. YZ would like to thank D Shaw and S Imaoka, ANSYS Inc. and K-H Kim for their valuable assistance.

References

[1] Yao J J 2000 RF MEMS from a device perspective *J. Micromech. Microeng.* **10** R9–39

[2] Yao Z J, Chen S, Eshelman S, Denniston D and Goldsmith C L 1999 Micromechined low-loss microwave switches *J. Microelectromech. Syst.* **8** 129–34

[3] Peroulis D, Sarabandi K and Katehi L P B 2002 Design of low actuation voltage RF MEMS switches *IEEE MTT-S Int. Microwave Symp. Digest* pp 165–8

[4] Zavracky P M, Majumder S and McGruer N E 1997 Micromechanical switches fabricated using nickel surface micromachining *J. Microelectromech. Syst.* **6** 3–9

[5] Tan G-L and Rebeiz G M 2002 A DC-contact MEMS shunt switch *IEEE Microw. Wirel. Compon. Lett.* **12** 212–4

[6] Hosaka H, Kuwano H and Yanagisawa K 1994 Electromagnetic microrelays: concepts and fundamental characteristic *Sensors Actuators* A **40** 41–7

[7] Rebeiz G M 2003 *RF MEMS: Theory, Design and Technology* (Hoboken, NJ: Wiley)

[8] van Spengen W M, Puers R, Mertens R and De Wolf I 2003 A low frequency electrical test set-up for the reliability assessment of capacitive RF MEMS switches *J. Micromech. Microeng.* **13** 604–12

[9] Goldsmith C, Ehmke J, Malczewski A, Pollans B, Eschelman S, Yao Z, Brank J and Eberly M 2001 Life time characterization of capacitive RF MEMS switches *IEEE MTT-S Int. Microwave Symp. Digest* pp 227–30

[10] Zhu Y and Espinosa H D 2004 Reliability of capacitive RF MEMS switches at high and low temperatures *Int. J. RF Microw. Comput.-Aided Eng.* **14** 317–28

[11] Mercado L L, Lee T Y T, Kuo S M and Amrine C 2003 Thermal solutions for discrete and wafer-level RF MEMS switch packages *IEEE Trans. Adv. Packag.* **26** 318–26

[12] Lafontan X, Le Touze C, Wenk B, Kolesnik I, Pressecq F, Perez G, Nicot J-M, Dardalhon M and Rigo S 2002 Environmental test bench for reliability studies: influence of the temperature on RF switches with metallic membranes *Proc. SPIE* **4755** 624

[13] Rizk J B, Chaiban E and Rebeiz G M 2002 Steady state thermal analysis and high-power reliability considerations of RF MEMS capacitive switches *IEEE MTT-S Digest* pp 239–42

[14] Jensen B D, Saitou K, Volakis J L and Kurabayashi K 2003 Fully integrated electrothermal multidomain modeling of RF MEMS switches *IEEE Microw. Wirel. Compon. Lett.* **13** 364–6

[15] Chauffleur X, Rabbia L, Pons P, Grenier K, Plana R and Dantas L 2002 Effect of membrane shape on mechanical behavior of RF switches *Tech. Digest, 16th Euro. Conf. on Solid-State Transducers* pp 92–5

[16] Espinosa H D, Zhu Y, Fischer M and Hutchinson J 2003 An experimental/computational approach to identify moduli and residual stress in MEMS RF-switches *Exp. Mech.* **43** 309–16

[17] Li G and Aluru N R 2001 Linear, nonlinear and mixed-regime analysis of electrostatic MEMS *Sensors Actuators* A **91** 278–91

[18] Gould P L 1988 *Analysis of Shells and Plates* (New York: Springer)

[19] Osterberg P M and Senturia S D 1997 M-test: a test chip for MEMS material property measurement using electrostatically actuated test structures *J. Microelectromech. Syst.* **6** 107–18

[20] Hung E S and Senturia S D 1999 Extending the travel range of analog-tuned electrostatic actuators *J. Microelectromech. Syst.* **8** 497–505

[21] Chen S, Baughn T V, Yao Z J and Goldsmith C L 2002 A new *in situ* residual stress measurement method for a MEMS thin fixed-fixed beam structure *J. Microelectromech. Syst.* **11** 309–16

[22] Fischer M 1999 MEMS material testing *Master of Science Thesis* Purdue University

[23] Rabinov V L, Gupta R J and Senturia S D 1997 The effect of release etch-holes on the electromechanical behavior of MEMS structures *Tech. Digest, 1997 Int. Conf. on Solid-State Sensors and Actuators* pp 1125–8

[24] Espinosa H D, Fischer M, Zhu Y and Lee S 2001 3D computational modeling of RF MEMS switches *Tech. Digest, Int. Conf. on Modeling and Simulation of Microsystems* pp 402–5

[25] Randall J N and Kao M-Y *USA Patent no* 6100477

[26] van Mullem C J, Gabriel K J and Fujita H 1991 Large deflection performance of surface micromachined corrugated diaphragms *Proc. Transducers'91* pp 1014–7